Analysis and Optimization of Clutch Judder based on Hybrid Uncertain Model with Random and Interval Variables

Y. D. Hao[1], Z. C. He[1*], G. Y. Li[1*], Eric Li[2], YY Huang[3], CC Liang[3]

[1]*State Key Laboratory of Advanced Design and Manufacturing for Vehicle Body, Hunan University, Changsha, 410082 P. R. China*

[2] *School of Science, Engineering & Design, Teesside University, Middlesbrough, UK*

[3]*Technology Development Cneter, SAIC GM Wuling Automobile Co., Ltd, Liuzhou, Peoples's Republic of China*

Abstract

The clutch judder has serious impacts on the NVH (noise, vibration and harshness) performance. In this paper, a simplified four-degree-of-freedom dynamic model with nonlinear friction torque and engine torque excitation is developed to simulate the clutch judder, and the stability and dynamic response of the clutch is analyzed based on the simplified model. In addition, the real part of judder modal frequency, the moment when the clutch enters the stick state, and the fluctuation level of the driving part of clutch are treated as the evaluation indexes of the judder performance. An uncertain hybrid model with random and interval variables is used to described the uncertainty of parameters and a hybrid perturbation vertex method is formulated to compute the uncertainty of the clutch judder. Furthermore, the parameters with high sensitivities are used as design variables and the uncertainty-based optimization are conducted to reduce the clutch judder. The optimization results have strongly validated that the proposed method is very effective to improve the robustness of the clutch judder performance.

***Key words*:** Driveline, Judder, Hybrid Uncertainty Model, Random variables, Interval variables

* Corresponding author. Tel. /fax: +86 73188822051.

E-mail address: hezhicheng815@163.com (Z. C. He), gyli@hnu.cn (G. Y. Li)

1 Introduction

The clutch is one of the most important parts in automobile driveline. Its role is to enable the smooth engagement and temporary separation between the engine and the transmission. A clutch includes the driving and driven parts, as shown in Fig. 1. The engine power is delivered through the friction moment between the driving part and driven part. In the process of automobile start, there exists a low-frequency vibration with the gradual engagement of driving and driven parts. This phenomenon often causes the longitudinal vibration of automobile body, which is known as the clutch judder. The clutch judder has serious impacts on the NVH (noise, vibration and harshness) performance, especially in start process.

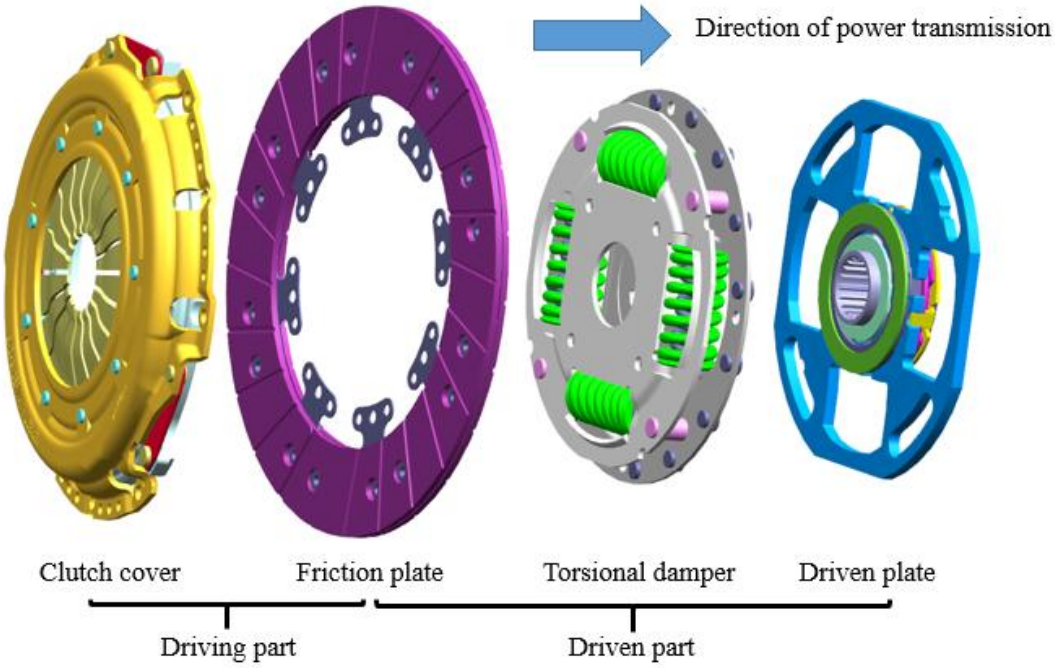

Fig. 1: The structure of automobile clutch

The clutch judder was first demonstrated by Jarvis and Oldershaw in 1973 [1]. Some possible causes of clutch judder were discussed in their study. The self-excitation of the friction moment during the process of the clutch engagement was proved to be the main source of clutch judder [2-4]. Yang et al. presented a simplified three-degree-of-freedom dynamic model with nonlinear friction torque and identified the effect of the engine excitation on clutch judder [5]. The effect of frictional lining material was studied by Li et al. [6]. They prepared 18 kinds of

frictional lining specimens in order to investigate their performance in judder resistance and establish a relationship between judder behavior and material parameters. Ma et al. mentioned that the clutch judder was influenced by the non-uniformity of the interface contact pressure distribution, which was excited by frictionally induced thermal load [7]. In addition, different models are developed to simulate the judder oscillations. Bartlett and Whalley employed hybrid modelling techniques in the investigation of the dynamic performance of ‘long’ driveshafts, which include a clutch and load, for power transmission purposes [8]. The nonlinear clutch model was analyzed by Centea et al. and the effect of various clutch systems and driveline components were studied [9]. Häfele and Küçükay built a multi-body dynamic model to analyze the different mechanisms of judder [10]. The control of the clutch judder was also studied in the past twenty years. Rabeih and Crolla showed that it was possible in principle to avoid clutch judder problems by controlling the clutch modulation using robust and adaptive control algorithms [11]. Naus et al. presented the design and implementation of a robust control concept to actively damp judder in a clutch system [12]. Sando et al. proposed a method to suppress the clutch judder with H∞ Control [13].

However, all these studies are based on the deterministic model. To our best knowledge, there is no systematic study using uncertainty-based design and optimization to reduce the clutch judder. In fact, the uncertainties of clutch and driveline parameters are inescapable. There always exists a vast quantity of uncertainties arising from the clutch and driveline system itself, as well as the environmental and operational conditions. These uncertainties may cause the system performance to change or fluctuate, such as the clutch judder. Hence it is necessary to analyze the clutch judder performance with consideration of uncertainty.

There are many uncertain models to describe the uncertainty parameters, such as probability model [14], interval model [15] and convex model [16]. Different uncertain models are used to describe different kinds of parameters. As the uncertainties of the stiffness and inertia parameters in the clutch judder model are mainly caused by manufacture errors, the probability model is more appropriate. As

the mechanism of damping is not clear yet and the values of the damping parameters can only be determined by experience and references [17, 18], the interval model is suitable for the damping parameters. Hence a hybrid uncertain model used in many other fields [19-22] with both random and interval variables to describe the uncertainty of the clutch judder is developed in this work. In the development of hybrid uncertain model, the real part of judder modal, the moment when the clutch enters the stick state, and the fluctuation level of the driving part of clutch are treated as the evaluation indexes of the judder performance. The parameters with high sensitivities are used as the design variables and the uncertainty-based optimization are conducted to reduce the clutch judder.

The paper is outlined as follows. The clutch judder model and the friction moment in the clutch engagement process are formulated in Section 2. In Section 3, the stability and dynamic responses of the judder are analyzed and the evaluation indexes of clutch judder are presented. The uncertain analysis and optimization methods based on the hybrid uncertain model with random and interval variables are presented in Section 4. Some concluding remarks are made in the last Section.

2 Formulation of the clutch judder model in the clutch engaging process

2.1 Dynamic model of clutch judder

In this study, a front engine and front wheel drive SUV (sports utility vehicle) is used as simple automobile. The engine of the SUV is a 4-cylinder and 4-stroke turbocharged engine with 1.5L engine displacements. A dry friction diaphragm clutch and a 5 gear manual transmission are equipped.

The driveline judder is a low frequency vibration occurred at the vehicle start-up process. The acting frequency is low and the excitation source of the driveline judder is the self-excitation of the friction moment. Hence the transmission, drive shafts, rear-axle, wheels have little influence on the driveline judder, which are ignored in this work. Therefore, a simplified driveline model with 4 DOFs (degrees of freedom) model is developed as shown in Fig. 2. The details of the parameters employed in the simulation are shown in Table 1.

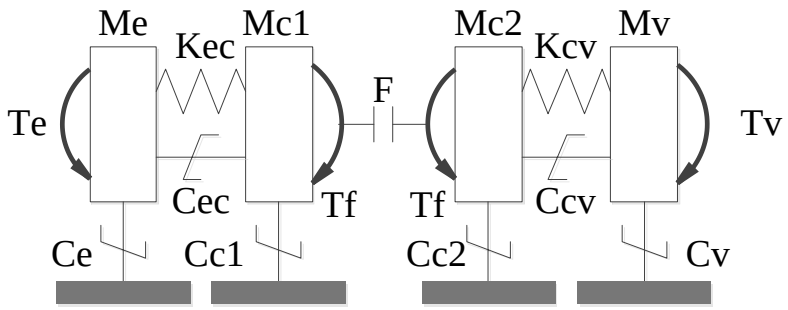

Fig. 2: Simulation model of driveline judder

Table 2: The parameters in the driveline judder model

Me	Inertia of the engine (exclude flywheel)	Ce	Damping of the engine
Mc1	Inertia of flywheel and driving part of clutch	Cc1	Damping of the driving part of clutch
Mc2	Inertia of driven part of clutch	Cc2	Damping of the driven part of clutch
Mv	Inertia of the whole driveline (exclude engine and clutch)	Cv	Damping of the driveline
Kec	Torsional stiffness between the engine and the flywheel	Te	Engine output torque
Kcv	Torsional stiffness of the clutch torsional vibration damper	Tf	Friction moment
Cec	Torsional damping between the engine and the flywheel	Tv	Driveline equivalent resistance moment
Ccv	Torsional damping of the clutch torsional vibration damper	F	Pressing force of the clutch

There are three states when the clutch is at work: separation, stick and slip. In the separation state, the driving part of the clutch is separated with the driven part. Therefore, there is no friction moment between the two parts. In the stick state, the driven part synchronously rotates with the driving part and the relative speed is zero. While it is in the slip state, there exists a relative rotation speed between the two parts of the clutch. It is obvious that the judder never happens in the separation state.

Let θ_e, θ_{c1}, θ_{c2} and θ_v denote the rotational displacement of the engine, driving part of clutch, driven part of the clutch and driveline, respectively. In the slip state, the kinetic energy, potential energy and dissipated energy of the system can be computed by

$$E = \frac{1}{2}M_e\dot{\theta}_e^2 + \frac{1}{2}M_{c1}\dot{\theta}_{c1}^2 + \frac{1}{2}M_{c2}\dot{\theta}_{c2}^2 + \frac{1}{2}M_v\dot{\theta}_v^2$$

$$U = \frac{1}{2}K_{ec}(\theta_{c1} - \theta_e)^2 + \frac{1}{2}K_{cv}(\theta_v - \theta_{c2})^2 \qquad \text{Slip state} \qquad (1)$$

$$D=\frac{1}{2}C_{ec}(\dot{\theta}_{c1}-\dot{\theta}_e)^2+\frac{1}{2}C_{cv}(\dot{\theta}_v-\dot{\theta}_{c2})^2+\frac{1}{2}C_e\dot{\theta}_e^2+\frac{1}{2}C_{c1}\dot{\theta}_{c1}^2$$
$$+\frac{1}{2}C_{c2}\dot{\theta}_{c2}^2+\frac{1}{2}C_v\dot{\theta}_v^2$$

In the stick state, the driving part of the clutch has the same rotating speed with the driven part. Hence $\theta_c=\theta_{c1}=\theta_{c2}$. The energy equations can be expressed as

$$E=\frac{1}{2}M_e\dot{\theta}_e^2+\frac{1}{2}(M_{c1}+M_{c2})\dot{\theta}_c^2+\frac{1}{2}M_v\dot{\theta}_v^2$$
$$U=\frac{1}{2}K_{ec}(\theta_c-\theta_e)^2+\frac{1}{2}K_{cv}(\theta_v-\theta_c)^2$$
$$D=\frac{1}{2}C_{ec}(\dot{\theta}_c-\dot{\theta}_e)^2+\frac{1}{2}C_{cv}(\dot{\theta}_v-\dot{\theta}_c)^2+\frac{1}{2}C_e\dot{\theta}_e^2 \quad \text{Stick state} \quad (2)$$
$$+\frac{1}{2}(C_{c1}+C_{c2})\dot{\theta}_c^2+\frac{1}{2}C_v\dot{\theta}_v^2$$

Applying Eqs. (1) and (2) to the Lagrange Equation, the dynamical equation of the driveline judder can be obtained as

$$\begin{cases} M_e\ddot{\theta}_e+C_e\dot{\theta}_e+C_{ec}(\dot{\theta}_e-\dot{\theta}_{c1})+\mathrm{K}_{ec}(\theta_e-\theta_{c1})=\mathrm{T}_e \\ M_{c1}\ddot{\theta}_{c1}+C_{c1}\dot{\theta}_{c1}+C_{ec}(\dot{\theta}_{c1}-\dot{\theta}_e)+\mathrm{K}_{ec}(\theta_{c1}-\theta_e)=-\mathrm{T}_f \\ M_{c2}\ddot{\theta}_{c2}+C_{c2}\dot{\theta}_{c2}+C_{cv}(\dot{\theta}_{c2}-\dot{\theta}_v)+\mathrm{K}_{cv}(\theta_{c2}-\theta_v)=\mathrm{T}_f \\ M_v\ddot{\theta}_v+C_v\dot{\theta}_v+C_{cv}(\dot{\theta}_v-\dot{\theta}_{c2})+\mathrm{K}_{cv}(\theta_v-\theta_{c2})=\mathrm{T}_v \end{cases} \quad \text{Stick state} \quad (3)$$

$$\begin{cases} M_e\ddot{\theta}_e+C_e\dot{\theta}_e+C_{ec}(\dot{\theta}_e-\dot{\theta}_c)+\mathrm{K}_{ec}(\theta_e-\theta_c)=\mathrm{T}_e \\ (M_{c1}+M_{c2})\ddot{\theta}_c+(C_{c1}+C_{c2})\dot{\theta}_c+\mathrm{K}_{ec}(\theta_c-\theta_e)+ \\ \mathrm{K}_{cv}(\theta_c-\theta_v)+C_{ec}(\dot{\theta}_c-\dot{\theta}_e)+C_{cv}(\dot{\theta}_c-\dot{\theta}_v)=0 \\ M_v\ddot{\theta}_v+C_v\dot{\theta}_v+C_{cv}(\dot{\theta}_v-\dot{\theta}_c)+\mathrm{K}_{cv}(\theta_v-\theta_c)=\mathrm{T}_v \end{cases} \quad \text{Slip state} \quad (4)$$

The driveline equivalent resistance moment T_v is treated as a constant value. The engine output torque T_e can be expressed as follows:

$$T_e=T_0+T_2\sin\omega_e t \quad (5)$$

where t denotes the time, ω_e is the fire frequency , T_0 and T_2 are 0 order and 2nd order torque of the engine. As the model is only used to analyze the judder in the low frequency, the high orders of the output torque of the engine are ignored.

2.2 The friction moment in the clutch engaging process

When the clutch is at work, there always exists a friction moment between the driving part and the driven part. The friction moment is related with the relative rotation speed v. When the driven part synchronously rotates with the driving part, the relative rotation speed $v=0$. The friction moment T_f can be expressed as follows:

$$T_f = \begin{cases} T_l & |T_l| \le T_{\max} \\ T_{\max}\,\mathrm{sign}(\mathrm{T}_l) & |T_l| > T_{\max} \end{cases} \tag{5}$$

where T_l denotes the transmitted torque when the clutch is completely engaged, and $T_{\max}$ is the maximum static friction moment.

$T_{\max}$ can be computed by Coulomb's friction law

$$T_{\max} = \mu_0 z R_m F \tag{6}$$

where μ_0 denotes the static friction coefficient, z represents the number of the friction face, F is the pressing force acting on the friction face, and R_m is the equivalent friction radius. Let R_o and R_i be the outer and inner radius of the friction plate. R_m is given as follows:

$$R_m = \frac{2(\mathrm{R}_o^{\,3} - \mathrm{R}_i^{\,3})}{3(\mathrm{R}_o^{\,2} - \mathrm{R}_i^{\,2})} \tag{7}$$

T_l can be obtained by the mechanical analysis of the model in Fig. 2. Applying Newton's Second Law to the driven part of the clutch, the following equation is obtained:

$$T_{l1} = -M_{c1}\ddot{\theta}_{c1} - \mathrm{C}_{c1}\dot{\theta}_{c1} + K_{ec}(\theta_e - \theta_{c1}) + C_{ec}(\dot{\theta}_e - \dot{\theta}_{c1}) \tag{8}$$

When the driving part is used as the analytic target in the mechanical analysis, T_l can be obtained

$$T_{l2} = M_{c2}\ddot{\theta}_{c2} + \mathrm{C}_{c2}\dot{\theta}_{c2} + K_{cv}(\theta_{c2} - \theta_v) + C_{cv}(\dot{\theta}_{c2} - \dot{\theta}_v) \tag{9}$$

In practical computation, there is a tiny difference between T_{l1} and T_{l2}. Hence T_l

can be obtained by the average of T_{l1} and T_{l2}

$$T_l = \frac{T_{l1} + T_{l2}}{2} \tag{10}$$

When the clutch works at slip state, the relative rotation speed between the driving part and the driven part v is not equal to zero, the friction moment can be computed by

$$T_f = \mu z R_m F sign(v) \tag{11}$$

where μ denotes the dynamic friction coefficient.

The dynamic friction coefficient μ is related with the temperature T, the pressing force F and the relative rotation speed v. It is very difficult to obtain the precise expression of μ. Several friction models have been proposed in the past 30 years [23~24]. In this study, the Stribeck model [25] is used and the friction coefficient is simplified as a linear model. The relationship between the dynamic friction coefficient and the relative rotation speed can be expressed as

$$\mu = \mu_0 + m_\mu |v| \tag{12}$$

where m_μ denotes the dynamic friction coefficient gradient.

Applying Eq. (12) to Eq. (11), the friction moment can be given as follows:

$$T_f = (\mu_0 + m_\mu |v|) z R_m F sign(\mathrm{v}) \tag{13}$$

Combine Eqs. (5) and (13), the friction moment of the clutch can be expressed

$$T_f = \begin{cases} (\mu_0 + m_\mu |v|) z R_m F sign(v) & v \neq 0 \\ T_l & v = 0, |T_l| \leq T_{\max} \\ T_{\max}\, \mathrm{sign}(\mathrm{T}_l) & v = 0, |T_l| > T_{\max} \end{cases} \tag{14}$$

2.3 The united form of judder dynamic equation

It can be seen from Eqs. (3) and (4) that the dynamic equation is different in the slip and stick states. However, as Eq. (14) is applied, the dynamic equation of the driveline judder can be unified as Eq. (4). Rewrite Eq. (4) into the matrix form:

$$\mathbf{M}\ddot{\boldsymbol{\theta}} + \mathbf{C}\dot{\boldsymbol{\theta}} + \mathbf{K}\boldsymbol{\theta} = \mathbf{T} \tag{15}$$

where

$$\boldsymbol{\theta} = [\theta_e \quad \theta_{c1} \quad \theta_{c2} \quad \theta_v]^T \tag{16}$$

$$\mathbf{M} = \begin{bmatrix} M_e & 0 & 0 & 0 \\ 0 & M_{c1} & 0 & 0 \\ 0 & 0 & M_{c2} & 0 \\ 0 & 0 & 0 & M_v \end{bmatrix} \tag{17}$$

$$\mathbf{C} = \begin{bmatrix} C_e + C_{ec} & -C_{ec} & 0 & 0 \\ -C_{ec} & C_{c1} + C_{ec} & 0 & 0 \\ 0 & 0 & C_{c2} + C_{cv} & -C_{cv} \\ 0 & 0 & -C_{cv} & C_{cv} + C_v \end{bmatrix} \tag{18}$$

$$\mathbf{K} = \begin{bmatrix} K_{ec} & -K_{ec} & 0 & 0 \\ -K_{ec} & K_{ec} & 0 & 0 \\ 0 & 0 & K_{cv} & -K_{cv} \\ 0 & 0 & -K_{cv} & K_{cv} \end{bmatrix} \tag{19}$$

$$\mathbf{T} = [T_e \quad -T_f \quad T_f \quad T_v]^T \tag{20}$$

The variation of the pressing force F is also considered. In the process of clutch engaging, F increases gradually to the maximum value with the time. The maximum value and rising process of pressing force F are determined by the axial stiffness of the waveform piece. In this study, the axial stiffness of the waveform piece is treated as a constant value. The time behavior of F is written as

$$F = \begin{cases} F_0(\dfrac{t}{t_0}) & 0 \le t < t_0 \\ F_0 & t > t_0 \end{cases} \tag{21}$$

where F_0 is the maximum pressing force of the waveform piece, t_0 denotes the time of the waveform piece compression. t_0 is determined by the axial stiffness of the waveform piece κ_w and the axial velocity of the waveform piece v_w.

$$t_0 = \frac{F_0}{\kappa_w v_w} \tag{22}$$

The values of the parameters are all listed in Table 2.

Table 2: The parameter values in the driveline judder model

Parameter	Values	Parameter	Values

M_e	0.045 $kg \cdot m^2$	R_o	0.125 m
M_{c1}	0.092 $kg \cdot m^2$	R_i	0.085 m
M_{c2}	0.012 $kg \cdot m^2$	z	2
M_v	2.5 $kg \cdot m^2$	μ_0	0.27
C_e	0.05 $Nm \cdot s / rad$	T_0	110 Nm
C_{c1}	0.01 $Nm \cdot s / rad$	T_2	130 Nm
C_{c2}	0.01 $Nm \cdot s / rad$	ω_e	150 rad / s
C_v	0.10 $Nm \cdot s / rad$	T_v	70 Nm
C_{ec}	0.05 $Nm \cdot s / rad$	m_μ	-0.00025
C_{cv}	0.05 $Nm \cdot s / rad$	F_0	3700 N
K_{ec}	24743.24 Nm / rad	κ_w	5200 N / mm
K_{cv}	739.12 Nm / rad	ν_w	5 mm / s

3 Driveline judder analysis

3.1 Stability analysis of the driveline judder

The stability analysis is able to predict the critical occurrence of the driveline judder [26]. Transform Eq. (15) and move the item which contains the relative rotation speed $|v|$ in T_f to the left side of the equal sign. Combine the moving part with the damping matrix, Eq. (15) becomes

$$\mathbf{M}\ddot{\boldsymbol{\theta}} + \mathbf{C}'\dot{\boldsymbol{\theta}} + \mathbf{K}\boldsymbol{\theta} = \mathbf{T}' \tag{23}$$

in which the mass matrix $\mathbf{M}$ and the stiffness matrix $\mathbf{K}$ are the same as those in Eq. (15), and the damping matrix $\mathbf{C}'$ can be expressed as

$$\mathbf{C}' = \begin{bmatrix} C_e + C_{ec} & -C_{ec} & 0 & 0 \\ -C_{ec} & C_{c1} + C_{ec} + C_\mu & -C_\mu & 0 \\ 0 & -C_\mu & C_{c2} + C_{cv} + C_\mu & -C_{cv} \\ 0 & 0 & -C_{cv} & C_{cv} + C_v \end{bmatrix} \tag{24}$$

where C_μ denotes the damping item which come from T_f. C_μ can be computed by

$$C_\mu = m_\mu z R_m F \tag{25}$$

Let $\mathbf{X} = \left[\theta_e \quad \theta_{c1} \quad \theta_{c2} \quad \theta_v \quad \dot{\theta}_e \quad \dot{\theta}_{c1} \quad \dot{\theta}_{c2} \quad \dot{\theta}_v\right]^T$ and rewrite Eq. (23) in the following form

$$\dot{\mathbf{X}} = \mathbf{AX} + \mathbf{BU} \tag{26}$$

where

$$\mathbf{A} = \begin{bmatrix} \mathbf{0} & \mathbf{I} \\ -\mathbf{M}^{-1}\mathbf{K} & -\mathbf{M}^{-1}\mathbf{C}' \end{bmatrix} \tag{27}$$

$$\mathbf{B} = \begin{bmatrix} \mathbf{0} & \mathbf{0} \\ \mathbf{0} & \mathbf{M}^{-1} \end{bmatrix} \tag{28}$$

$$\mathbf{U} = \begin{bmatrix} \mathbf{0} \\ \mathbf{T}' \end{bmatrix} \tag{29}$$

Based on Lyapunov stability theory [27], the system stability can be judged by the eigenvalues of the state matrix $\mathbf{A}$. When the real part of the eigenvalues is negative, the system is stable. Otherwise, the system is unstable. As the real part increases, the degree of judder stability improves with it. Apply the numerical values in Table 2 to the Eq. (27) and evaluate the matrix eigenvalues. The eigenfrequency of the driveline judder model is $39.58\,Hz$, and the real part of the eigenvalue is 5.64. Hence the driveline judder system is unstable due to positive eigenvalues.

Next, the influence of dynamic friction coefficient gradient m_μ, damping coefficient of clutch torsional vibration damper C_v and damping coefficient of clutch driving part C_{c2} is studied. Fig. 3 shows the relationship between the real parts of the eigenvalues and the values of m_μ, C_v, C_{c2}.

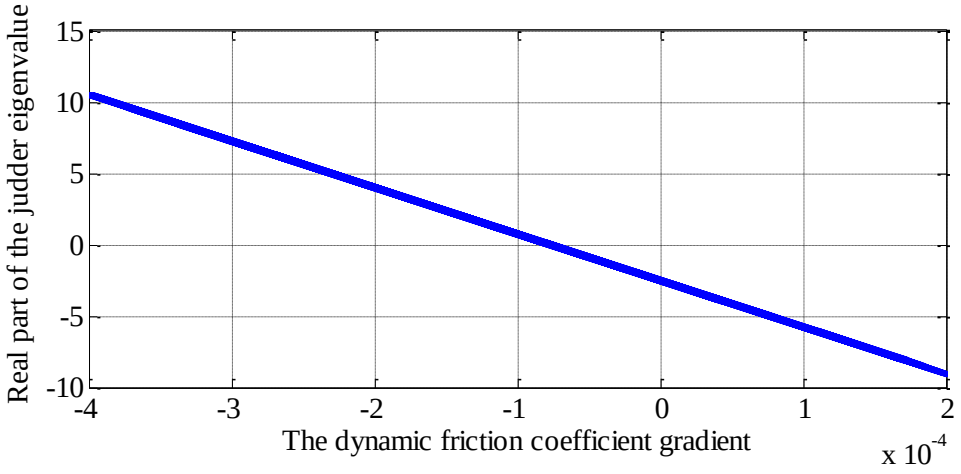

(a) The influence of the dynamic friction coefficient gradient

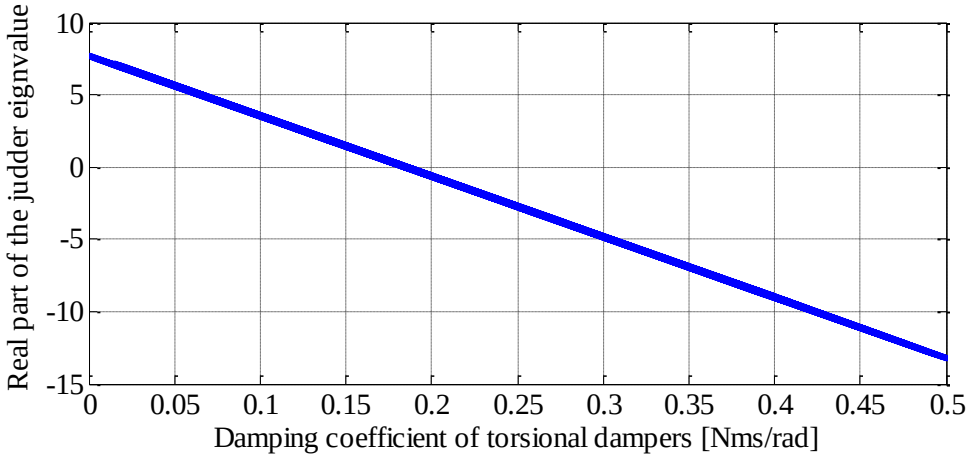

(b) The influence of the damping coefficient of clutch torsional vibration damper

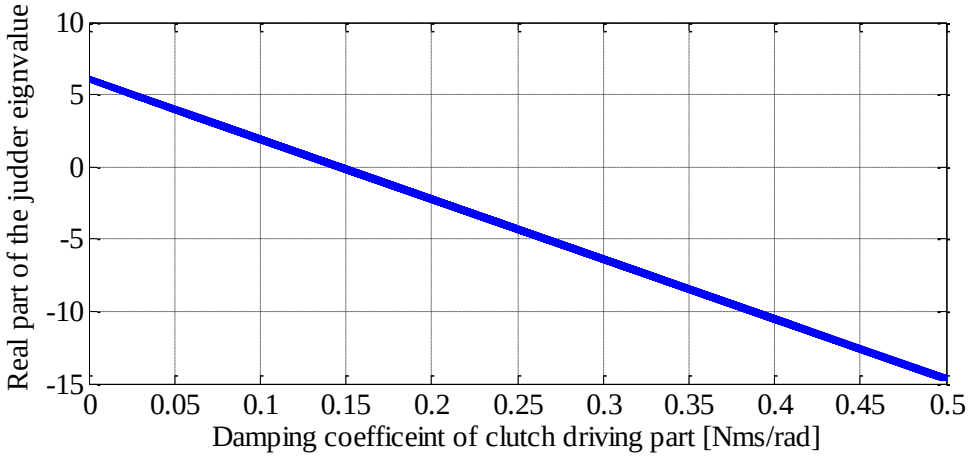

(c) The influence of the damping coefficient of clutch driving part

Fig. 3: The influence of system parameters on the stability

It can be seen from Fig. 3 that the stability of the driveline judder scales linearly with the dynamic friction coefficient gradient, damping coefficient of clutch torsional

vibration damper and damping coefficient of clutch driving part. As the friction coefficient gradient and damping coefficients decrease, the real parts of the judder eigenvalue increase with it. Thus, the system becomes more unstable. In order to improve the system stability, the dynamic friction coefficient gradient, the damping coefficient of clutch torsional vibration damper and the clutch driving part should be decreased.

3.2 Dynamic response analysis of the driveline judder

Based on Eq. (15), the state equation of judder system can be written as

$$\begin{cases} \mathbf{X} = \mathbf{A}\mathbf{X} + \mathbf{B}\mathbf{U} \\ \mathbf{X}(0) = \mathbf{X}_0 \end{cases} \tag{30}$$

where

$$\mathbf{X} = \left[\theta_e \quad \theta_{c1} \quad \theta_{c2} \quad \theta_v \quad \dot{\theta}_e \quad \dot{\theta}_{c1} \quad \dot{\theta}_{c2} \quad \dot{\theta}_v \right]^T \tag{31}$$

$$\mathbf{A} = \begin{bmatrix} \mathbf{0} & \mathbf{I} \\ -\mathbf{M}^{-1}\mathbf{K} & -\mathbf{M}^{-1}\mathbf{C} \end{bmatrix} \tag{32}$$

$$\mathbf{B} = \begin{bmatrix} \mathbf{0} & \mathbf{0} \\ \mathbf{0} & \mathbf{M}^{-1} \end{bmatrix} \tag{33}$$

$$\mathbf{U} = \left[\mathbf{0} \quad \mathbf{T} \right]^T \tag{34}$$

It is noted that the excitation vector $\mathbf{T}$ is time variant. Thus, the work state of the clutch must be known before solving excitation vector $\mathbf{T}$. The judgment of the work state is determined by the relative rotation speed $|v|$. It is noted that the relative rotation speed $|v|$ will fluctuate nearby zero, which leads to misconvergence of the numerical results.

In order to guarantee the accuracy and convergence of the computation, Karnopp friction model is employed in the process of the friction moment [28]. A tiny tolerance dv is defined in the Karnopp friction model. When the relative rotation speed $|v| \le dv$, the system is considered at the stick state and the friction moment is computed by Eq. (5). Otherwise, Eq. (13) is used to compute the friction moment. Apply the Karnopp friction model, the friction moment equation between the driven

and driving part of the clutch in Eq. (14) can be transformed as

$$T_f = \begin{cases} (\mu_0 + m_\mu |v|) z R_m F sign(v) & |v| \geq dv \\ T_l & |v| < dv, |T_l| \leq T_{\max} \\ T_{\max} \operatorname{sign}(T_l) & |v| < dv, |T_l| > T_{\max} \end{cases} \tag{35}$$

Four-order Range-Kuttle method [29] is used to solve Eq. (30). The time step is set as 0.0002s. The initial rotation speed at engine and driven part of clutch is set as 600 rad/s. While the initial rotation speed at driving part of clutch and driveline is determined by 200 rad/s. At each iteration, the friction moment is recomputed by Eq. (35). As shown in Fig. 4, the variation of the angular velocity at driven and driving part of the clutch is presented.

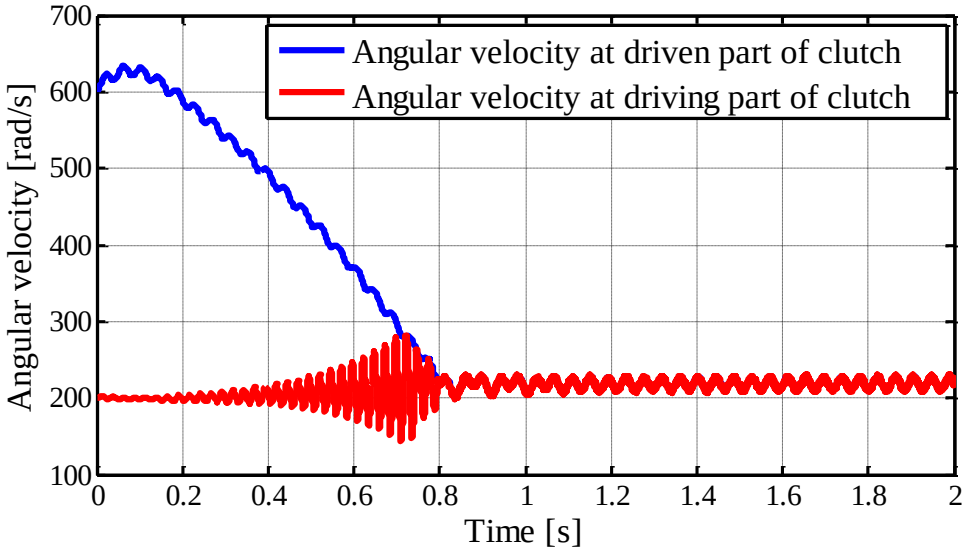

Fig. 4: The angular velocity at driven and driving part of clutch

It can be seen from Fig. 4 that before 0.8s, the angular velocities at driven and driving part of clutch become close to each other. At about 0.8s, the clutch comes to the stick state and the driven and driving parts of clutch rotate synchronously. In this process, the dramatic fluctuations of the driving part of clutch are the major cause of driveline judder.

Except the real part of judder eigenvalue, the driveline judder also can be evaluated by the fluctuation level of the driving part of clutch. The fluctuation level can be quantified by the sum of deviation between the instantaneous speed and the average speed. The sum of deviation is defined as the fluctuation index, which can be expressed as

$$F_{fluc} = \sqrt{\frac{1}{N}\sum_{n=1}^{N}[\dot{\theta}_{c2(\mathrm{n})} - \mathrm{m}_{\theta c2}]^2} \tag{36}$$

in which N is the number of moments at slip state, $\dot{\theta}_{c2(\mathrm{n})}$ and $\mathrm{m}_{\theta c2}$ denote the instantaneous speed and average speed of the driving part of clutch. The larger the fluctuation index is, the larger the fluctuation level of the driving part of clutch is.

The moment when the clutch becomes the stick state is also an important index, which determines the response speed of clutch at starting and shift process and has an obvious influence on the driving feeling. Therefore, this moment must be considered in the driveline design and optimization.

4 Robust-based design optimization of driveline judder

4.1 Random and interval hybrid model of driveline judder

As the driveline design parameters and parameters can be obtained by structural analysis, the normal probability distribution is used to describe their uncertainties. However, it is very hard to obtain the distribution characteristic of the parameters based on experience. Hence the interval model is presented to describe their uncertainties. For engine exciting and resistance moment, their values are changed by the working conditions. Therefore, their uncertainties can also be described by the interval model. The uncertain models for all parameters are listed in Table 3.

It is seen that there are 24 parameters in Table 3. The computational time will be very huge if all parameters are treated as the uncertain variables. Hence it is necessary to analyze the sensitivities of the parameters with respect to the driveline judder. Only the key parameters with high sensitivities are treated as the uncertain variables.

Table 3: Sources and uncertain models of driveline judder parameters

Parameter	Source	Uncertain model	Parameter	Source	Uncertain model
M_e	Structural analysis	Probability model	R_o	Design parameter	Probability model
M_{c1}	Structural analysis	Probability model	R_i	Design parameter	Probability model
M_{c2}	Structural analysis	Probability model	z	Design parameter	-

M_v	Structural analysis	Probability model	μ_0	Estimated value	Interval model
C_e	Estimated value	Interval model	T_0	Change with working condition	Interval model
C_{c1}	Estimated value	Interval model	T_2	Change with working condition	Interval model
C_{c2}	Estimated value	Interval model	ω_e	Change with working condition	Interval model
C_v	Estimated value	Interval model	T_v	Change with working condition	Interval model
C_{ec}	Estimated value	Interval model	m_μ	Estimated value	Interval model
C_{cv}	Estimated value	Interval model	F_0	Design parameter	Probability model
K_{ec}	Structural analysis	Probability model	κ_w	Design parameter	Probability model
K_{cv}	Design parameter	Probability model	ν_w	Estimated value	Interval model

The real part of judder eigenvalue R_p, the moment when the clutch enters the stick state t_s, and the fluctuation index of the clutch driving part Fl_c, are the three evaluation indexes to evaluate the driveline judder. The sensitivity of parameter x can be computed by

$$s_x = \beta \left| \frac{g(\mathrm{x}+\Delta \mathrm{x}) - g(\mathrm{x})}{\Delta x} \right| \tag{37}$$

in which Δx is a micro-increment of x, $g(\mathrm{x})$ denotes the evaluation index of driveline judder, and β stands for scale factor. For different evaluation indexes, β can take different values.

The sensitivities of the random parameters and interval parameters are listed in Table 4 and Table 5, respectively.

Table 4: Sensitivities results of random parameters

Parameter	R_p	t_s	Fl_c
M_e	**0.01**	**21.60**	**226.33**
M_{c1}	**0.00**	**23.80**	**363.22**

M_{c2}	**437.83**	**4.80**	**4737.31**
M_v	0.02	0.00	0.59
K_{ec}	0.00	0.00	0.00
K_{cv}	0.00	0.00	0.35
R_o	**42.80**	**22.00**	**8.29**
R_i	**33.11**	**20.40**	**8.40**
F_0	0.00	0.00	0.01
κ_w	**0.00**	**24.00**	**345.99**

Table 5: Sensitivities results of interval parameters

Parameter	R_p	t_s	Fl_c
C_{ec}	0.00	0.00	0.13
C_{cv}	**41.87**	**46.60**	**751.40**
C_e	**0.00**	**25.80**	**515.37**
C_{c1}	**0.00**	**25.80**	**515.42**
C_{c2}	**41.47**	**0.80**	**231.54**
C_v	0.00	0.80	36.45
μ_0	**0.00**	**19.80**	**366.50**
T_0	0.00	0.00	0.02
T_2	0.00	0.00	0.00
ω_e	0.00	0.00	0.03
T_v	0.00	0.00	0.03
m_μ	**1630.46**	**15.04**	**9451.71**

ν_w	0.00	0.00	0.02

From Table 4 and Table 5, it is known that there are 6 random parameters and 6 interval parameters with high sensitivities, which are shown in boldface in the tables and will be treated as the uncertain variables in the analysis and optimization of the driveline judder. M_e, M_{c1}, M_{c2}, R_o, R_i and κ_w are modeled by the probability theory and the expected values and standard deviations must be given. While C_{cv}, C_e, C_{c1}, C_{c2}, μ_0 and m_μ are modeled by interval theory and the center values and interval radius should be given. The uncertain variables' expected values, standard deviations, center values and interval radius are determined by the accuracy of manufacture and engineering experience, as shown in Table 6.

Table 6: Parameters of uncertain models for uncertain variables

Random variables	Expected values	Standard deviations	Interval parameters	Center value	Interval radius
M_e	0.045	0.00113	C_{cv}	0.05	0.02
M_{c1}	0.092	0.0023	C_e	0.05	0.02
M_{c2}	0.012	0.0003	C_{c1}	0.01	0.004
R_o	0.125	0.00313	C_{c2}	0.01	0.004
R_i	0.085	0.00213	μ_0	0.27	0.02
κ_w	5200	130	m_μ	-2.5E-4	0.3E-4

4.2 Hybrid perturbation vertex method for the driveline judder

The uncertain model of the driveline judder proposed in this study is a random and interval hybrid model. As the computational cost using Monte Carlo Method [30] and Hybrid Perturbation Monte Carlo Method [31] is extremely expensive, the Hybrid Perturbation Vertex Method (HPVM) is employed to analyze the upper and lower bounds of the expected values and standard deviations of the driveline judder uncertainty model.

The driveline judder uncertainty model has 6 random variables and 6 interval

variables. Let $\mathbf{a}$ denote the vector formed by random variables and $\mathbf{b}$ denote the vector formed by interval variables. We have

$$\begin{cases} \mathbf{a} = [M_e \quad M_{c1} \quad M_{c2} \quad R_o \quad R_i \quad \kappa_w]^T \\ \mathbf{b} = [C_{cv} \quad C_e \quad C_{c1} \quad C_{c2} \quad \mu_0 \quad m_\mu]^T \end{cases} \tag{38}$$

$Exp(\mathbf{a})$ and $Sd(\mathbf{a})$ represent the vectors made up by the expected values and the standard deviations of all elements in vector $\mathbf{a}$, respectively. $\overline{\mathbf{b}}$ and $\underline{\mathbf{b}}$ are the vectors made up by the upper and lower bounds of all elements in vector $\mathbf{b}$, respectively. The center value vector $\mathbf{b}^c$, the interval radius vector $|\Delta\mathbf{b}|$ and the perturbation interval matrix $\Delta\mathbf{b}$ can be expressed as

$$\begin{cases} \mathbf{b} = (\overline{\mathbf{b}} + \underline{\mathbf{b}})/2 \\ |\Delta\mathbf{b}| = (\overline{\mathbf{b}} - \underline{\mathbf{b}})/2 \\ \Delta\mathbf{b} = [\mathbf{b} - \underline{\mathbf{b}} \quad \mathbf{b} + \overline{\mathbf{b}}] \end{cases} \tag{39}$$

Let $\mathbf{F}$ be the response vector of driveline judder. $\mathbf{F}$ is a function about $\mathbf{a}$ and $\mathbf{b}$.

$$\mathbf{F}(\mathbf{a},\mathbf{b}) = [F_1 \quad F_2 \quad F_3]^T \tag{40}$$

where F_1, F_2 and F_3 denote the real part of judder eigenvalue R_p, the moment when the clutch is at stick state t_s, and the fluctuation index of clutch driving part Fl_c, respectively.

Firstly, the uncertainty of the interval variables $\mathbf{b}$ is ignored and regard it as a constant vector. Expand $\mathbf{F}(\mathbf{a},\mathbf{b})$ in the form of first order Taylor Series

$$\mathbf{F}(\mathbf{a},\mathbf{b}) \approx \mathbf{F}(\mathbf{a},\mathbf{b})\big|_{\mathbf{a}=Exp(\mathbf{a})} + \sum_{i=1}^{6} \left.\frac{\partial \mathbf{F}(\mathbf{a},\mathbf{b})}{\partial a_i}\right|_{\mathbf{a}=Exp(\mathbf{a})} (\mathrm{a}_i - \mathrm{Exp}(\mathrm{a}_i)) \tag{41}$$

Based on Eq. (3.41), ignore the uncertainty of interval variables $\mathbf{a}$ and regard it as a constant vector. $\mathbf{F}(\mathbf{a},\mathbf{b})$ can be further expanded based on $\mathbf{b}$ as

$$
\begin{aligned}
\mathbf{F}(\mathbf{a},\mathbf{b}) &\approx \mathbf{F}(\mathbf{a},\mathbf{b})\big|_{\mathbf{a}=Exp(\mathbf{a})} + \sum_{i=1}^{n} \left.\frac{\partial \mathbf{F}(\mathbf{a},\mathbf{b})}{\partial a_i}\right|_{\mathbf{a}=Exp(\mathbf{a})} (\mathrm{a}_i - \mathrm{Exp}(\mathrm{a}_i)) \\
&\approx \mathbf{F}(\mathbf{a},\mathbf{b})\Big|_{\substack{\mathbf{a}=Exp(\mathbf{a}) \\ \mathbf{b}=\mathbf{b}^c}}^{\mathbf{a}=Exp(\mathbf{a})} + \sum_{j=1}^{m} \left.\frac{\partial \mathbf{F}(\mathbf{a},\mathbf{b})}{\partial b_j}\right|_{\substack{\mathbf{a}=Exp(\mathbf{a}) \\ \mathbf{b}=\mathbf{b}^c}} \Delta b_j \\
&\quad + \sum_{i=1}^{n} \left.\frac{\partial \mathbf{F}(\mathbf{a},\mathbf{b})}{\partial a_i}\right|_{\mathbf{a}=Exp(\mathbf{a})} (\mathrm{a}_i - \mathrm{Exp}(\mathrm{a}_i)) \\
&\quad + \sum_{i=1}^{n}\sum_{j=1}^{m} \left.\frac{\partial^2 \mathbf{F}(\mathbf{a},\mathbf{b})}{\partial a_i \partial b_j}\right|_{\substack{\mathbf{a}=Exp(\mathbf{a}) \\ \mathbf{b}=\mathbf{b}^c}} (\mathrm{a}_i - \mathrm{Exp}(\mathrm{a}_i))\Delta b_j
\end{aligned}
\tag{42}
$$

where m and n are the number of random variables and interval variables, respectively. In this study, $m = n = 6$.

Eq. (42) can be written as

$$
\mathbf{F}(\mathbf{a},\mathbf{b}) \approx \mathbf{F}^c + \Delta\mathbf{F} \tag{43}
$$

where $\mathbf{F}^c$ is the value of $\mathbf{F}(\mathbf{a},\mathbf{b})$ when $\mathbf{a}$ and $\mathbf{b}$ obtain their expected values and center values, respectively, and $\Delta\mathbf{F}$ denotes the perturbation interval of $\mathbf{F}(\mathbf{a},\mathbf{b})$. $\mathbf{F}^c$ and $\Delta\mathbf{F}$ can be expressed as

$$
\mathbf{F}^c = \mathbf{F}(\mathbf{a},\mathbf{b})\Big|_{\substack{\mathbf{a}=Exp(\mathbf{a}) \\ \mathbf{b}=\mathbf{b}^c}}^{\mathbf{a}=Exp(\mathbf{a})} \tag{44}
$$

$$
\begin{aligned}
\Delta\mathbf{F} &= \sum_{j=1}^{m} \left.\frac{\partial \mathbf{F}(\mathbf{a},\mathbf{b})}{\partial b_j}\right|_{\substack{\mathbf{a}=Exp(\mathbf{a}) \\ \mathbf{b}=\mathbf{b}^c}} \Delta b_j + \sum_{i=1}^{n} \left.\frac{\partial \mathbf{F}(\mathbf{a},\mathbf{b})}{\partial a_i}\right|_{\mathbf{a}=Exp(\mathbf{a})} (\mathrm{a}_i - \mathrm{Exp}(\mathrm{a}_i)) \\
&\quad + \sum_{i=1}^{n}\sum_{j=1}^{m} \left.\frac{\partial^2 \mathbf{F}(\mathbf{a},\mathbf{b})}{\partial a_i \partial b_j}\right|_{\substack{\mathbf{a}=Exp(\mathbf{a}) \\ \mathbf{b}=\mathbf{b}^c}} (\mathrm{a}_i - \mathrm{Exp}(\mathrm{a}_i))\Delta b_j
\end{aligned}
\tag{45}
$$

Applying the random variable's moment function method to Eqs. (44) and (45), the expected value and standard deviation of $\mathbf{F}(\mathbf{a},\mathbf{b})$ can be expressed as

$$
Exp(\mathbf{F}) = \mathbf{F}(\mathbf{a},\mathbf{b}) + \sum_{j=1}^{m} \left.\frac{\partial \mathbf{F}(\mathbf{a},\mathbf{b})}{\partial b_j}\right|_{\substack{\mathbf{a}=Exp(\mathbf{a}) \\ \mathbf{b}=\mathbf{b}^c}} \Delta b_j \tag{46}
$$

$$
Sd(\mathbf{F}) = \sqrt{\sum_{i=1}^{n} \left[\left.\frac{\partial \mathbf{F}(\mathbf{a},\mathbf{b})}{\partial a_i}\right|_{\substack{\mathbf{a}=Exp(\mathbf{a}) \\ \mathbf{b}=\mathbf{b}^c}} + \sum_{j=1}^{m} \left.\frac{\partial^2 \mathbf{F}(\mathbf{a},\mathbf{b})}{\partial a_i \partial b_j}\right|_{\substack{\mathbf{a}=Exp(\mathbf{a}) \\ \mathbf{b}=\mathbf{b}^c}} \Delta b_j\right] \cdot Sd(\mathrm{a}_i)^2} \tag{47}
$$

The first-order and second-order partial derivatives in Eqs. (46) and (47) can be computed by numerical method

$$\begin{cases} \dfrac{\partial \mathbf{F}(\mathbf{a},\mathbf{b})}{\partial a_i} = \dfrac{\mathbf{F}(\mathbf{a}+\Delta_i,\mathbf{b})-\mathbf{F}(\mathbf{a},\mathbf{b})}{\Delta_i} \\ \dfrac{\partial \mathbf{F}(\mathbf{a},\mathbf{b})}{\partial b_j} = \dfrac{\mathbf{F}(\mathbf{a},\mathbf{b}+\boldsymbol{\Delta}_j)-\mathbf{F}(\mathbf{a},\mathbf{b})}{\Delta_j} \\ \dfrac{\partial^2 \mathbf{F}(\mathbf{a},\mathbf{b})}{\partial a_i \partial b_j} = \dfrac{\mathbf{F}(\mathbf{a}+\boldsymbol{\Delta}_i,\mathbf{b}+\boldsymbol{\Delta}_j)+\mathbf{F}(\mathbf{a},\mathbf{b})-\mathbf{F}(\mathbf{a}+\boldsymbol{\Delta}_i,\mathbf{b})-\mathbf{F}(\mathbf{a},\mathbf{b}+\boldsymbol{\Delta}_j)}{\Delta_i \Delta_j} \end{cases} \tag{48}$$

where Δ_i and Δ_j denote a vector where the i th and j th element is a micro-increment, respectively.

It is known from Eqs. (46) and (47) that the expected value and standard deviation of $\mathbf{F}(\mathbf{a},\mathbf{b})$ are functions of the interval variable Δb_j. The value of Δb_j can come from the lower bound $-\left|\Delta b_j\right|$ to the upper bound $\left|\Delta b_j\right|$. In Hybrid Perturbation Monte Carlo Method, the bounds of expected value and the standard deviation can be computed with Monte Carlo Method by

$$\begin{cases} Exp(\mathbf{F})_u = \max\limits_{\Delta b_j \in [-\left|\Delta b_j\right|,\left|\Delta b_j\right|]} \{\mathrm{Exp}(\mathbf{F})\} \\ Exp(\mathbf{F})_l = \min\limits_{\Delta b_j \in [-\left|\Delta b_j\right|,\left|\Delta b_j\right|]} \{\mathrm{Exp}(\mathbf{F})\} \end{cases} \tag{49}$$

$$\begin{cases} Sd(\mathbf{F})_u = \max\limits_{\Delta b_j \in [-\left|\Delta b_j\right|,\left|\Delta b_j\right|]} \{Sd(\mathbf{F})\} \\ Sd(\mathbf{F})_l = \min\limits_{\Delta b_j \in [-\left|\Delta b_j\right|,\left|\Delta b_j\right|]} \{Sd(\mathbf{F})\} \end{cases} \tag{50}$$

where $Exp(\mathbf{F})_u$ and $Exp(\mathbf{F})_l$ denote the upper and lower bound of the expected value of $\mathbf{F}(\mathbf{a},\mathbf{b})$, and $Sd(\mathbf{F})_u$ and $Sd(\mathbf{F})_l$ denote the upper and lower bound of the standard deviation of $\mathbf{F}(\mathbf{a},\mathbf{b})$.

From Eqs. (46) and (47), it is known that the $Exp(\mathbf{F})$ and $Sd(\mathbf{F})$ are monotone functions about Δb_j. Therefore, traverse all the vertex combinations of Δb_j and compute the expected values and standard diversions. The maximum and minimum must be the upper and lower bounds

$$\begin{cases} Exp(\mathbf{F})_u = \max\limits_{q=1,2,3,\mathrm{L}\ 2^m} \{\mathrm{Exp}(\mathbf{F})\} \\ Exp(\mathbf{F})_l = \min\limits_{q=1,2,3,\mathrm{L}\ 2^m} \{\mathrm{Exp}(\mathbf{F})\} \end{cases} \tag{51}$$

$$\begin{cases} Sd(\mathbf{F})_u = \max\limits_{q=1,2,3,\mathrm{L}\ 2^m} \{Var(\mathbf{F})\} \\ Sd(\mathbf{F})_l = \min\limits_{q=1,2,3,\mathrm{L}\ 2^m} \{Var(\mathbf{F})\} \end{cases} \tag{52}$$

where q is the number of the vertex combinations of Δb_j.

In a random and interval hybrid model with n interval variables, Eqs. (46) and (47) should be calculated for 2^n times. In this study, there are only 64 times of calculations, which is much smaller than Monte Carlo Method.

To sum up, the flow path of the uncertain numerical analysis with Hybrid Perturbation Vertex Method (HPVM) can be summarized as:

1. Expand $\mathbf{F}(\mathbf{a},\mathbf{b})$ to the form of first order Taylor Series as shown in Eq. (42), than $\mathbf{F}^c$ and $\Delta\mathbf{F}$ can be computed by Eqs. (44) and (45), respectively.

2. The expected value and standard deviation of $\mathbf{F}(\mathbf{a},\mathbf{b})$ are computed by Eqs. (46) and (47).

3. Through obtaining all the vertex combinations of Δb_j, 2^n combinations are generated.

4. Traversing all the vertex combinations of Δb_j, the upper and lower bounds of expected value of $\mathbf{F}(\mathbf{a},\mathbf{b})$ can be obtained by Eq. (51).

5. Traversing all the vertex combinations of Δb_j, the upper and lower bounds of standard deviation of $\mathbf{F}(\mathbf{a},\mathbf{b})$ can be obtained by Eq. (52).

The bounds of the expected value and the standard deviation using Hybrid Perturbation Vertex Method (HPVM) are listed in Table 7.

Table 7: Parameters of uncertain models for uncertain variables

	Expected value upper bound	Expected value lower bound	Standard deviation upper bound	Standard deviation lower bound

R_p	6.07	5.22	0.89	0.65
t_s	1.39	0.94	0.17	0.11
Fl_c	17.55	10.20	8.45	5.53

It can be seen from Table 7 that the standard deviation of the upper bound is very large. It means that the judder indexes are very sensitive to the values of driveline parameters. With slight change of the uncertain variables, there is a huge variance of judder indexes. Hence it is necessary to optimize the clutch judder performance based on robust-based design.

4.3 Robust-based design optimization based on hybrid perturbation vertex method

To simplify the optimization model, not every parameter in the judder model is treated as the design variable. In this study, four parameters including the inertia of driven part of clutch M_{c2}, the outer diameter of friction plate R_o, the inner diameter of friction plate R_i, and the axial stiffness of the waveform piece κ_w are used as the design variables. The ranges of the design variables in the optimization process are listed in Table 8.

Table 8: Ranges of design variables

Variable	Design value	Upper bound	Lower bound
M_{c2}	0.012	0.015	0.010
R_o	0.125	0.140	0.110
R_i	0.085	0.100	0.070
κ_w	5200	6500	4000

In hybrid perturbation method presented in this study, the bounds of the expected value and the standard deviation are obtained. Therefore, the traditional robust-based design optimization is not adaptive [32]. Hence a new robust-based optimization equation is formulated here to improve the driveline judder performance.

In traditional robust-based optimization, the objective function about the

expected value and the standard deviation is given as follows:

$$f(\mu_F(\mathbf{x}),\sigma_F(\mathbf{x}))=\frac{k\mu_F(\mathbf{x})}{w_\mu}+\frac{(1-\mathrm{k})\sigma_F(\mathbf{x})}{w_\sigma} \tag{53}$$

where $\mathbf{x}$ is the design variable vector, μ_F and σ_F are the expected value and the standard deviation, respectively, k is the weighting factor, w_μ and w_σ are the scaling factors.

In the optimization model based on random and interval parameters, the upper bounds of the expected value and the standard deviation are used to construct the objective function. The objective function in Eq. (53) can be expressed as

$$f(\bar{\mu}_F(\mathbf{x},\mathbf{a},\mathbf{b}),\bar{\sigma}_F(\mathbf{x},\mathbf{a},\mathbf{b}))=\frac{k\bar{\mu}_F(\mathbf{x},\mathbf{a},\mathbf{b})}{w_\mu}+\frac{(1-\mathrm{k})\bar{\sigma}_F(\mathbf{x},\mathbf{a},\mathbf{b})}{w_\sigma} \tag{54}$$

where $\mathbf{a}$ and $\mathbf{b}$ denote the random and interval parameter vectors, respectively.

The constraint condition can be also expressed by the upper bounds of expected value and standard deviation. In this study, the fluctuation index of clutch driving part is used as the objective function. The real part of judder eigenvalue R_p and the moment when the clutch enters the stick state are used as the constraint conditions. The robust-based optimization modal can be expressed as

$$\begin{cases} find & \mathbf{x} \\ \min & f(\mathrm{x},\mathrm{p})=f(\bar{\mu}_F(\mathbf{x},\mathbf{p}),\bar{\sigma}_F(\mathbf{x},\mathbf{p})) \\ s.t. & \bar{\mathbf{g}}(\mathbf{x},\mathbf{p})\le 0 \\ & \mathbf{x}^L\le\mathbf{x}\le\mathbf{x}^R \end{cases} \tag{55}$$

Multi-islands genetic algorithm is used to improve the driveline judder performance [33]. The optimization results of design variables are listed in Table 9. The uncertainties of the objective function and the constraint conditions are listed in Table 10. The rotation speed curves of clutch driven and driving parts after optimization are plotted in Fig. 5.

Table 9: Optimization results of design variables

Variable	Initial value	Optimal value	Variable	Initial value	Optimal value
M_{c2}	0.012	0.014	R_i	0.085	0.098

R_o	0.125	0.136	κ_w	5200	5617

Table 10: Optimization result of clutch judder indexes

		Real part of judder modal	Moment which clutch enters the stick state	Fluctuation index of the driving part of clutch
Upper bound of expected value	Initial value	6.07	1.39	17.55
	Optimal value	5.62	0.98	12.18
Lower bound of expected value	Initial value	5.22	0.94	10.20
	Optimal value	4.98	0.82	7.93
Upper bound of standard deviation	Initial value	0.89	0.17	8.45
	Optimal value	0.85	0.17	4.25
Lower bound of standard deviation	Initial value	0.65	0.11	5.33
	Optimal value	0.63	0.10	2.24

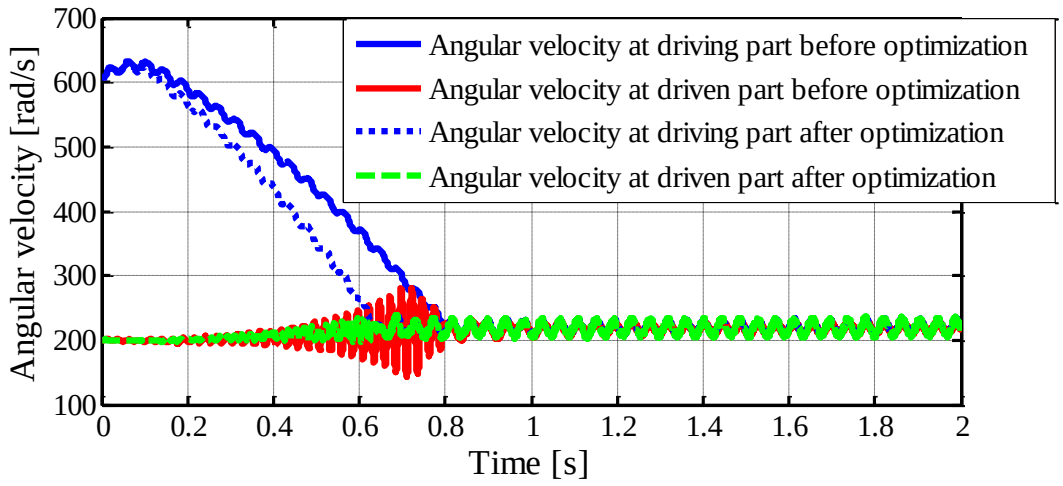

Fig. 5: The angular velocity at driven and driving part of clutch before and after optimization

From Table 10, it is obvious that the upper bounds of the expected values and the standard deviations of all the three indexes of the clutch judder are considerably below the initial values. Among them, the upper bound of standard deviation of fluctuation index is 50% lower than the initial value. Hence, the robustness of the optimal model is much better than the initial model. Fig. 5 shows that after optimization, the time when the clutch enters the stick state decreases obviously and the velocity fluctuation of the clutch driving part is reduced significantly. These numerical results have clearly demonstrated the effectiveness of the proposed method, which is very important in the practical application of design of the clutch judder.

5 Conclusions

In this work, a hybrid uncertain model with both random and interval variables is developed to analyze and optimize the performance of the clutch judder. In the proposed hybrid uncertainty model, the inertia and torsional parameters are descried by the normal distribution. While the damping and friction parameters, are modelled by the interval model. Three indexes including the real part of judder modal frequency, the moment when the clutch enters the stick state and the fluctuation level of the driving part of clutch, are used as the evaluated indexes of the clutch judder. Furthermore, a robust design optimization method based on hybrid uncertain model is also developed. The upper bounds of the expected values and the standard deviations of the judder indexes are used as objective function and boundary conditions. The results show that the model and method developed in this work are very effective to improve the robustness of the clutch judder.

References

[1] Jarvis, R. P., & Oldershaw, R. M. (1973). Clutch judder in automobile drivelines automobile division. ARCHIVE Proceedings of the Institution of Mechanical Engineers 1847-1982 (vols 1-196), 187(1973), 369-379.

[2] Morimura, H. (2003). Analysis of occurrence condition in clutch judder. Transactions of the Japan Society of Mechanical Engineers C, 69(682), 1543-1549.

[3] Zhang, J. 1. (2010). Study on clutch engagement judder during launch process for dual clutch transmissions. International Journal of Vehicle Noise & Vibration, 6(2/3/4), 176-199.

[4] Crowther, A., Zhang, N., Liu, D. K., & Jeyakumaran, J. K. (2004). Analysis and simulation of clutch engagement judder and stick-slip in automotive powertrain systems. Drive System Technique, 218(12), 1427-1446.

[5] Yang, L. K., Li, H. Y., Ahmadian, M., & Ma, B. (2015). Analysis of the influence of engine torque excitation on clutch judder. Journal of Vibration & Control, 14(3), 385-396.

[6] Li, T. C., Huang, Y. W., & Lin, J. F. (2015). Studies on centrifugal clutch judder behavior and the design of frictional lining materials. Mechanical Systems &

Signal Processing, 66.

[7] Ma, B., Yang, L., Li, H., & Lan, N. (2016). Hot judder behavior in multidisc clutches. ARCHIVE Proceedings of the Institution of Mechanical Engineers Part J Journal of Engineering Tribology 1994-1996 (vols 208-210).

[8] Bartlett, H., & Whalley, R. (1998). Power transmission system modelling. ARCHIVE Proceedings of the Institution of Mechanical Engineers Part C Journal of Mechanical Engineering Science 1989-1996 (vols 203-210), 212(6), 497-505.

[9] Centea, D., Rahnejat, H., & Menday, M. T. (2001). Non-linear multi-body dynamic analysis for the study of clutch torsional vibrations (judder). Applied Mathematical Modelling, 25(3), 177-192.

[10] Häfele, J., & Küçükay, F. (2014). Multi-body dynamics analysis of power train judder oscillations considering aggregate dynamics. International Journal of Vehicle Noise & Vibration, 10(1/2), 64-76.

[11] Rabeih, E. M. A., & Crolla, D. A. (1996). Intelligent control of clutch judder and shunt phenomena in vehicle drivelines. International Journal of Vehicle Design, 17(3), 318-332.

[12] Naus, G., Beenakkers, M., & Huisman, R. (2008). Robust control to suppress clutch judder.

[13] Sando, K., Yamamoto, T., Hashimoto, S., Shin, S., & Sawada, K. (2013). J101012 Clutch Judder Suppression with H∞ Control. Mechanical Engineering Congress, Japan (Vol.2013). The Japan Society of Mechanical Engineers.

[14] Gan, C. B., Wang, Y. H., Yang, S. X., & Cao, Y. L. (2013). Nonparametric modeling and vibration analysis of uncertain jeffcott rotor with disc offset. International Journal of Mechanical Sciences, 78(1), 126-134.

[15] Jiang, C., Ni, B. Y., Liu, N. Y., Han, X., & Liu, J. (2016). Interval process model and non-random vibration analysis. Journal of Sound & Vibration, 373, 104-131.

[16] Zhang, X. M., & Ding, H. (2008). Design optimization for dynamic response of vibration mechanical system with uncertain parameters using convex model. Journal of Sound & Vibration, 318(1–2), 406-415.

[17] Licari, J., Ugalde-Loo, C. E., Liang, J., Ekanayake, J., & Jenkins, N. (2012). Torsional damping considering both shaft and blade flexibilities. Wind Engineering, 36(2), 181-196.

[18] Macphail, R. A., & Snyder, R. G. (1989). Torsional damping and solvent friction in liquid n−butane: experimental estimates from raman spectroscopy. Journal of Chemical Physics, 91(7), 3895-3902.

[19] Xia, B., & Yu, D. (2013). An interval random perturbation method for structural-acoustic system with hybrid uncertain parameters. International Journal for Numerical Methods in Engineering, 97(3), 181-206.

[20] Chen, N., Yu, D., & Xia, B. (2016). Unified analysis approach for the energy flow in coupled vibrating systems with two types of hybrid uncertain parameters. Mechanical Systems & Signal Processing, 70–71, 542-556.

[21] Yadav, A. K., & Gaur, P. (2013). Robust adaptive speed control of uncertain hybrid electric vehicle using electronic throttle control with varying road grade. Nonlinear Dynamics, 76(1), 305-321.

[22] Zhang, W., Liu, J., Cho, C., & Han, X. (2015). A hybrid parameter identification method based on bayesian approach and interval analysis for uncertain structures. Mechanical Systems & Signal Processing, 60–61, 853-865.

[23] Todd, M. J., & Johnson, K. L. (1987). A model for coulomb torque hysteresis in ball bearings. International Journal of Mechanical Sciences, 29(5), 339-354.

[24] Feng, C., & Cui, Z. (2015). A 3-d model for void evolution in viscous materials under large compressive deformation. International Journal of Plasticity, 74, 192-212.

[25] Liu, Y., Pavlovskaia, E., Hendry, D., & Wiercigroch, M. (2013). Vibro-impact responses of capsule system with various friction models. International Journal of Mechanical Sciences, 72(72), 39-54.

[26] Pagola, F. L., Perez-Arriaga, I. J., & Verghese, G. C. (1989). On sensitivities, residues and participations: applications to oscillatory stability analysis and control. IEEE Transactions on Power Systems, 4(1), 278-285.

[27] Yoshikawa, T. (2009). Lyapunov stability theory. Veterinary Surgery, 44(4),

494–500.

[28] Ravanbod-Shirazi, L. (2003). Friction identification using the karnopp model, applied to an electropneumatic actuator. Proceedings of the Institution of Mechanical Engineers Part I Journal of Systems & Control Engineering, 217(2), 123-138.

[29] Dzhashitov, V. E., Pankratov, V. M., Golikov, A. V., Nikolaev, S. G., Kolevatov, A. P., & Plotnikov, A. D., et al. (2015). Erratum to: “hierarchical thermal models of fog_based strapdown inertial navigation system”. Gyroscopy and Navigation, 6(2), 156-156.

[30] Nakatani, J., Konno, K., & Moriguchi, Y. (2017). Variability-based optimal design for robust plastic recycling systems. Resources Conservation & Recycling, 116, 53-60.

[31] Gao, W., Wu, D., Song, C., Tin-Loi, F., & Li, X. (2011). Hybrid probabilistic interval analysis of bar structures with uncertainty using a mixed perturbation Monte-Carlo method. Finite Elements in Analysis & Design, 47(7), 643-652.

[32] Ishibuchi, H., Tanaka, H., (1990). Multiobjective programming in optimization of the interval objective function. European Journal of Operational Research, 48(2), 219-225.

[33] Hu, X., Chen, X., Zhao, Y., & Yao, W. (2014). Optimization design of satellite separation systems based on multi-island genetic algorithm. Advances in Space Research, 53(5), 870-876.